small methods
www.small-methods.com

High-Throughput Synthesis and Machine Learning Assisted Design of Photodegradable Hydrogels

Maximilian Seifermann, Patrick Reiser, Pascal Friederich, and Pavel A. Levkin**

Due to the large chemical space, the design of functional and responsive soft materials poses many challenges but also offers a wide range of opportunities in terms of the scope of possible properties. Herein, an experimental workflow for miniaturized combinatorial high-throughput screening of functional hydrogel libraries is reported. The data created from the analysis of the photodegradation process of more than 900 different types of hydrogel pads are used to train a machine learning model for automated decision making. Through iterative model optimization based on Bayesian optimization, a substantial improvement in response properties is achieved and thus expanded the scope of material properties obtainable within the chemical space of hydrogels in the study. It is therefore demonstrated that the potential of combining miniaturized high-throughput experiments with smart optimization algorithms for cost and time efficient optimization of materials properties.

1. Introduction

One of the key features material science is often trying to mimic is the ability of biological systems to respond to external stimuli. There is a necessity for an ongoing signal-response relation between a material and its environment when full control of complex processes such as the behavior of cells/tissue is required, the higher the amount of control the more complex the relation needs to be.[1] While advantages in material design are rapid, systems responding to various stimuli at once or in a complex manner are scarce and usually consist of a combination of different materials.[2] This multimaterial approach requires a large amount of materials to choose from in order to tailor the exact properties needed. While theoretically possible, producing the required amount of data in traditional fashion is not feasible, not least due to the enormous consumption of materials required for this as well as the processing of the sheer amount of data produced from it.

Throughout the last decade, machine learning (ML) methods[3] have proven useful in many research areas such as material science,[4–7] chemistry,[8–11] biology,[12–15] and drug discovery.[16–19] One major advantage of machine learning methods is the utilization of the vast amount of data generated in decades of research to achieve faster progress in science, e.g. by improving the virtual design of materials,[20] speeding up optimization processes[21–23] or yielding a better understanding of hidden relations in data and thus fundamental processes.[24–27] With continuing progress in ML research, the research speed of manual lab experiments and thus the generation of new data is not sufficient any longer to sustain the amounts of data needed to efficiently make use of new ML methods. Thus, increasing the throughput of experimental pipelines comes as a logical consequence and drives the research community to parallelize experiments in order to speed up data generation. Due to the increased need of reagents, consumables and effort to achieve this in a conventional and manual fashion, automated high-throughput platforms and miniaturization are becoming of central importance.

Experimental as well as computational HT-techniques are already commonly used to screen for potential drug candidates and can help identify potent inhibitors to treat diseases such as malaria or PVB19 infections.[28,29] Experimental workflows utilizing high-throughput concepts are becoming more sophisticated, thriving from simple viability-based readouts to allow more complex insights into biological systems and the fundamental dogma of biology while maintaining the advantages that came along with

M. Seifermann, P. A. Levkin
Institute of Biological and Chemical Systems-Functional Molecular Systems
Karlsruhe Institute of Technology
Hermann-von-Helmholtz-Platz 1, 76344 Eggenstein-Leopoldshafen, Germany
E-mail: levkin@kit.edu
P. Reiser, P. Friederich
Institute of Nanotechnology
Karlsruhe Institute of Technology
Hermann-von-Helmholtz-Platz 1, 76344 Eggenstein-Leopoldshafen, Germany
E-mail: pascal.friederich@kit.edu
P. Reiser, P. Friederich
Institute of Theoretical Informatics
Karlsruhe Institute of Technology
Am Fasanengarten 5, 76131 Karlsruhe, Germany
P. A. Levkin
Institute of Organic Chemistry
Karlsruhe Institute of Technology
Fritz-Haber-Weg 6, Karlsruhe, Germany

The ORCID identification number(s) for the author(s) of this article can be found under https://doi.org/10.1002/smtd.202300553

DOI: 10.1002/smtd.202300553

HT screening.[30–32] Miniaturization is not just a logical consequence of the economical consideration that experiments on a macroscopic scale consume more time and materials compared to a microscopical approach, but also a consequence of our own responsibility as researchers to minimize resource consumption as much as possible to allow sustainable scientific progression. Thus, miniaturization techniques need to develop further, away from the purely pharmacological or biological application, to fit the need of all research areas, especially the chemistry and material science-related ones, to allow resource-conserving ways of driving science forward.

In this study, we report a high-throughput methodology based on miniaturized experiments and machine learning for accelerated materials property optimization. We apply it to synthesize a library of ≈1000 hydrogels with different binary compositions, based on the combination of acrylic and methacrylic monomers and crosslinkers. We investigate their respective properties, in particular photostability. Hydrogels as an exemplary material class for screening were chosen due to their large chemical space as well as their promising nature as biocompatible biomaterials of the future and thus a broad field of potential applications. Due to the high water content integrated into a polymeric network, they strongly resemble tissue and extracellular matrix´s properties, making them promising candidate materials for biomedical engineering, soft robotics, tissue engineering, and microfluidics.[33–36] Multimaterials systems of photodegradable hydrogels are of particular interest for encapsulation and controlled release of cargo, such as drugs or cells, or for the creation of degradable scaffolds for 3D cell culture.[37]

In previous reports, we investigated inherently photodegradable hydro- and organogels based on methacrylate monomers and crosslinkers without the need of photosensitizing groups,[38] which have been proven applicable, e.g., in 3D cell culture.[39] Since their degradation speed was shown to be highly dependent on the polarity of the monomers and the crosslinking density, an evaluation of a variety of combinations can cover a large area of desired material properties.

We use the droplet microarray (DMA) as a platform for miniaturized high-throughput experiments.[40] The DMA is an array of hydrophilic spots on a superhydrophobic background created by photolithography.[41] It has proven as a potent platform for miniaturized chemistry and biology.[42,43] Combinatorial library synthesis through a polymer-based solid-phase synthesis strategy to achieve a synthesis of various structural motives has been realized and demonstrated for on-chip synthesis and screening.[44,45] Our experimental synthesis workflow is based on the preparation of sub-microliter-sized hydrogels in the hydrophilic spots of DMA.[40] For the analysis of those gels we use a noncontact method to measure UV-light-induced time-dependent degradation of soft polymers on a sub-microliter scale through fluorescence microscopy. The subsequent application of automated image analysis methods for the detection and measurement of pad size and intensity reduced manual work of characterization to a minimum and maximized the achievable throughput.

We demonstrate that by combining miniaturized high-throughput screening methods with machine learning based decision-making algorithms, we achieve an optimization of materials properties in a high-dimensional materials space of ≈13 440 possible hydrogels within 13 experiments, consuming in total only 0.65 mL of stock solution and less than 170 mg (836 µMol) of monomer and crosslinker materials. After the initial screening of 918 materials, the ML-guided approach allows us to expand the space of achievable combinations of pad size, intensity, and degradation speed significantly with just additional 79 new material compositions.

2. Results and Discussion

The experimental workflow established in this work consumes minimal amounts of materials and is suitable for broad parameter variation while maintaining good comparability of individual experiments on it, to maximize the data output in a limited set of experiments for potential use in machine learning. We choose a combinatorial approach to material synthesis to allow for a high variety of structural motives and investigate the behavior of the final material as a function of structural composition. With the chemical compositions, the solvent, the ratio between monomers and crosslinkers and the pH value, we have a huge set of independently variable parameters to achieve a maximum of different gel property combinations between the swelling/size and degradation speed.

For the miniaturized preparation of the hydrogel pads a nanoparticle-coated glass substrate modified with hydrophilic spots confined by superhydrophobic borders was used. These droplet microarrays were fabricated by photolithography, using UV-induced thiol-ene click reaction between surface vinyl-groups and either mercaptoethanol (hydrophilic) or 1*H*,1*H*,2*H*,2*H*-perfluorodecanethiol (PFDT) (hydrophobic). The final array had a format of 14 columns and 48 rows of hydrophilic 1 mm squares on a 2.5 cm × 7.5 cm microscopy glass slide. Here we achieve an experimental density of more than 35 experiments, requiring just 130 nL solutions each, per square centimeter, more than tenfold the density of standard 384 well plates. Additionally, the hydrophilic surface also leads to liquids dispensed into every spot to fully spread across the confined area, leading to a homogeneous geometry for all droplets even at volumes down to 10 nL.

To set the parameters for the later screening, a pipeline had to be developed and fully optimized. The critical steps involved: Stock solution preparation, dispensing step, polymerization, staining, degradation, and readout (**Figure 1**). For the preparation of the sub-microliter-sized droplets a Gyger Certus liquid dispensing system was used. Monomer stock solutions with low viscosity were required to guarantee high dispensing accuracy. To fit this need stock solutions with molarity between 1.66 M (for Monomers) and 0.58 M (for crosslinkers) were chosen. To set a parameter for comparison between the different experiments' monomer and cross-linker solution concentrations were chosen as a fixed parameter and only the molar ratio between monomer and crosslinker was varied.

Based on our group's previous work the model system chosen for optimization were different copolymers of poly(ethylene glycol)methacrylate (*M*w = 500 Da) (PEGMA 500) and [2-(methacryloyloxy)-ethyl]dimethyl-(3-sulfopropyl) ammonium hydroxide (SAMA), crosslinked by poly(ethylene glycol)dimethacrylate (*M*w = 750 Da) (PEGDMA 750) together with an oxygen scavenger system based on glucose oxidase (2.3 µM) and glucose (5.8 mM), which has been investigated on the DMA (**Figure 2**A).[8] First step to investigate was the polymerization

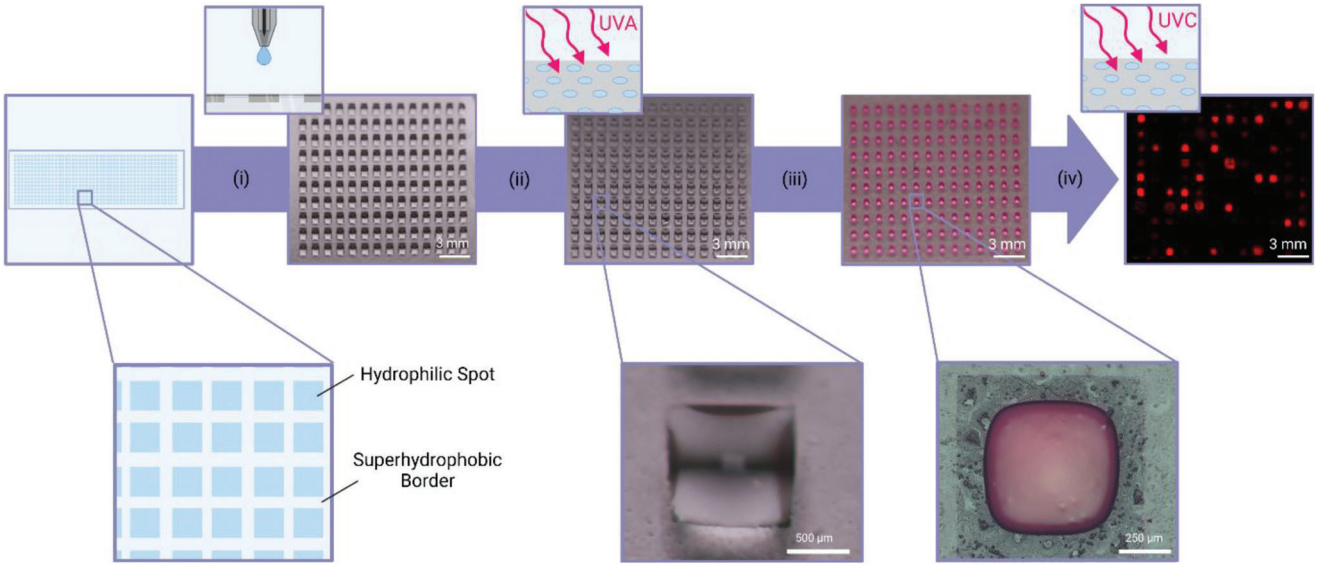

Figure 1. Schematic depiction of the experimental workflow to synthesize and screen sub-microliter-sized photodegradable hydrogels. For the synthesis of sub-microliter-sized hydrogel pads we used a droplet microarray, an array of 672 hydrophilic squares (1 × 1 mm) surrounded by superhydrophobic borders on the area of a standard glass microscopy slide. i) Solutions of initiator (lithium phenyl-2,4,6-trimethylbenzoylphosphinate) and oxygen scavenger (glucose oxidase) (30 nL), acrylate/methacrylate monomers (70 nL) and acrylate/methacrylate-based crosslinkers (30 nL) are dispensed into each spot to reach a final volume of 130 nL. ii) These prepolymerization solutions were sealed to suppress evaporation and then polymerized via photopolymerization at 365 nm for 30 min to yield transparent gel pads. iii) The gel pads are swollen in Rhodamine 6G solution to allow reliable visualization. The image below shows a gel pad of the same type on 1 mm spots, recorded with a digital microscope. iv) Stained gels then undergo cycles of UV irradiation (200–280 nm) and fluorescence microscopy to monitor their respective degradation courses with respect to their pad size and intensity.

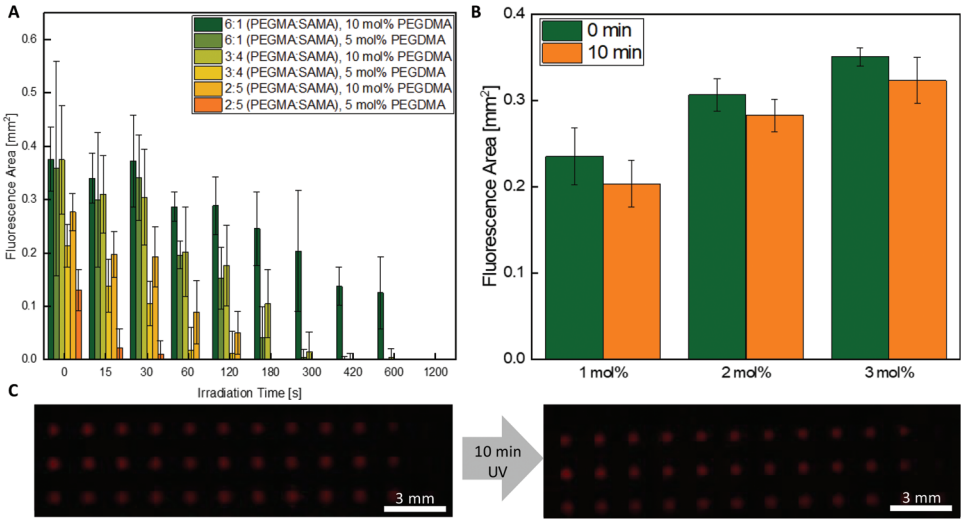

Figure 2. Experiments to adjust and control the parameters for later screening. A) Measured fluorescence area of a series of different hydrogel pads consisting of poly(ethylene glycol) methacrylate (Mw = 500 Da) (PEGMA) and [2-(methacryloyloxy)-ethyl]dimethyl-(3-sulfopropyl) ammonium hydroxide (SAMA) with different PEGMA:SAMA ratios and different amounts of poly(ethylene glycol) dimethacrylate (Mw = 750 Da) (PEGDMA) as crosslinker through the course of 20 min irradiation with UVC light. After swelling in Rhodamine 6G overnight, the gels were irradiated with UVC light (11.5 mW cm^{-2}, 200–280 nm) and measured by fluorescence microscopy successively. Values were acquired by continuous measurements on the same slide. Error bars show the standard deviation between 10 replicates each. B) Evaluation of gel stability under the influence of rhodamine 6G as a possible photosensitizer, to make sure the staining does not induce degradability. Nondegrading hydrogels made from poly(ethylene glycol) acrylate (*Mw* = 480 Da) and different amounts (in mol%) of poly(ethylene glycol) diacrylate (*Mw* = 700 Da) were irradiated for 10 min after incubation with rhodamine 6G overnight and afterward the change in fluorescence area was compared to check for degradation. Error bars are the standard deviation between 12 replicates. C) Fluorescence microscopy images of nondegradable hydrogels on 1 mm spots stained with rhodamine 6G.

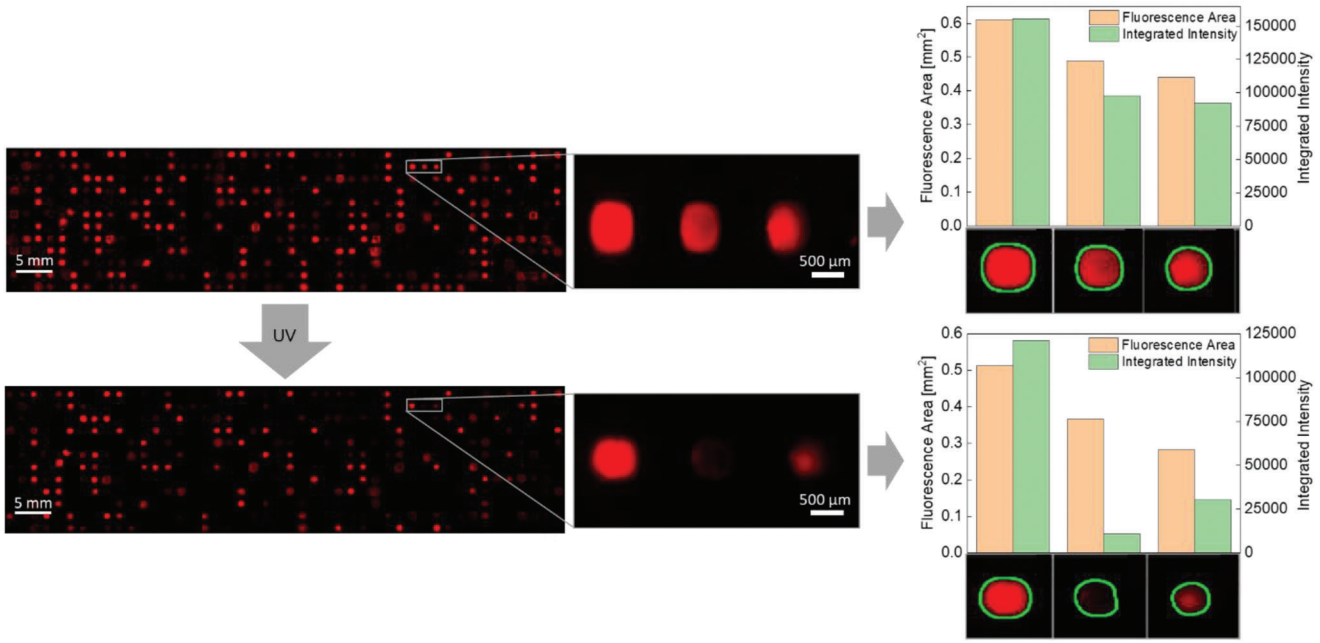

Figure 3. Example of a randomized layout of 92 different hydrogels with 6 repetitions each. Images were recorded on a fluorescence microscope at 570 nm excitation after 0 s (top) and 1200 s (bottom) irradiation with UVC light. Spots containing hydrogels are fluorescent, spots that did not yield hydrogel pads show no fluorescence. Magnified regions show a set of 3 different hydrogel pads with their respective border detected via edge detection as well as the respective fluorescence area and integrated intensity measured for each pad (right).

time. For this, hydrogels with different PEGMA:SAMA molar ratio (6:1 to 3:4) crosslinked with 10 mol% PEGDMA were polymerized on a scale of 130 nL per gel pad. Different intensities (5.41 – 18.0 mW cm^{-2}) and polymerization times (15 – 30 min) were investigated to find suitable polymerization time. For each condition, 2 sets of gels were polymerized, one set was directly stained with Rhodamine 6G and imaged, the other was irradiated an additional 2 min with UVC light before being submerged into Rhodamine 6G solution and imaged. Incompletely polymerized gels would still contain amounts of monomer, leading to a stagnation in the degradation curves or even an increase in size, whereas fully polymerized gels would only experience UV light-induced degradation, leading to a decrease in size. Suitable conditions would yield homogeneous pads that respond to irradiation with a decrease in size. Based on the highest decrease in pad size during the first 60 s of UVC-induced degradation and the formation of stable, homogeneous polymer pads, 30 min polymerization time at 5.41 mW cm^{-2} were considered optimal (Figure S3, Supporting Information).

Since the irradiation was performed under oxygen atmosphere, the influence of reactive oxygen species due to the photosensitizing properties of the dye in the mixture needed to be evaluated, to make sure all degradation processes were material properties and not induced through photosensitizing compounds. Nondegradable polymer compositions that were chemically similar to our model material with the only difference being the substitution of degradable methacrylate groups by acrylates were polymerized under the same conditions. These poly(ethylene glycol) acrylate-co-poly(ethylene glycol) diacrylate (PEGA-co-PEGDA) hydrogels were stained the same way, by submerging and swelling in an aqueous rhodamine 6G solution, and the change in size after 15 min irradiation with UVC light compared to the starting value after swelling was measured. The comparison of the final value and the end-point showed no significant decrease in the hydrogel's fluorescence area, indicating that the dye did not enable additional degradation mechanisms under the used conditions, making it suitable for the analysis of degradation behaviors (Figure 2B).

To test the overall robustness of the experimental workflow with unknown compositions beyond our characterized model system, 92 different binary compositions of 23 monomers and 4 crosslinkers ranging from 5 to 15 mol% (w.r.t monomer) were printed onto a slide according to our standardized protocol (**Figure 3**). For every composition, six repetitions were randomly distributed throughout the slide to obtain information about process variances and to avoid unwanted bias effects due to potential external influences due to substrate inhomogeneities. After polymerization and swelling, slides were closed and sealed with a UVC transmitting quartz glass slide on a PDMS frame to prevent evaporation during the irradiation and imaging steps. Characterization of UV degradation started by imaging the slides through fluorescence microscopy, followed by cycles of irradiation with UVC light and microscopy imaging. The final images were evaluated using an automated image processing protocol and each droplet's fluorescence area as well as the integrated pixel intensity were calculated. By this, the degradation curves for these gels were recorded three times on three different slides and showed good reproducibility and reliable results (Figure S4, Supporting Information), enabling the progression to the final screening. Following our experimental routine, we screened >900 compositions and recorded the respective degradation curves (**Figure 4**). More precisely, we performed measurements of 918 hydrogel

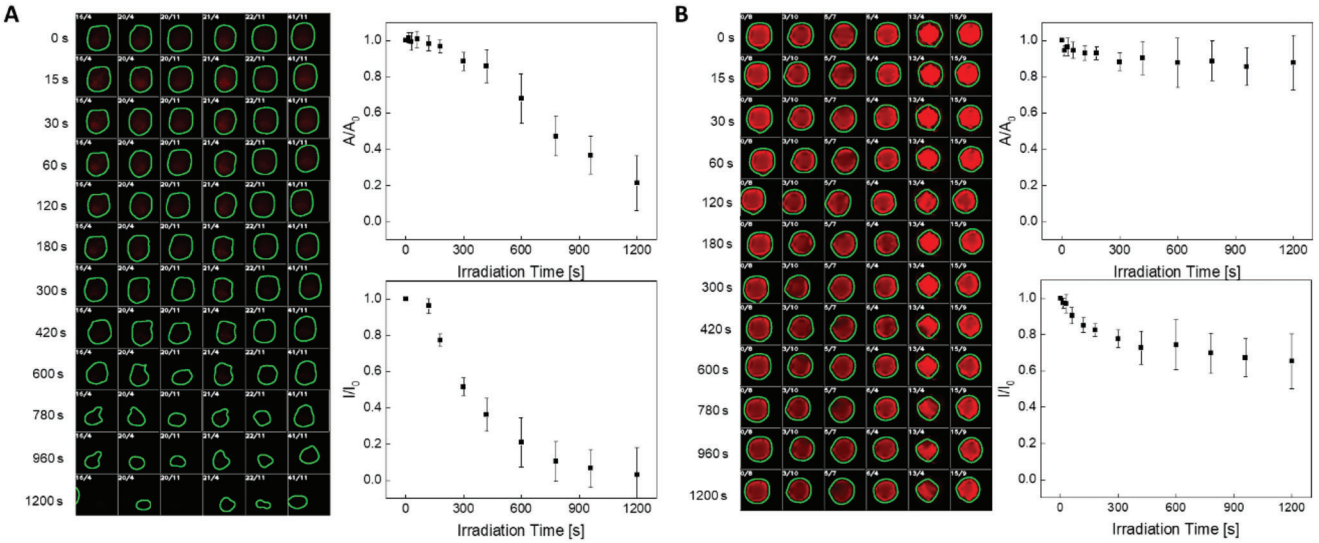

Figure 4. Two different sets of sub-microliter-sized hydrogel pads throughout the irradiation process, each row shows the 6 repetitions together with their relative position on the array (white number, row/column). The graphs show the relative fluorescence area (area within recognized borders) and integrated fluorescence area (sum of pixel intensity within the recognized border) of each repetition over the course of 20 min UVC irradiation. Values were calculated as the mean of the individual spot's values normalized to the starting value of the respective spot. Error bars are the standard deviation between all replicates. Hydrogels consist of A) 2-hydroxyethyl methacrylate, crosslinked with 8.5 mol% 1,4-butanediol diacrylate and B) 2-hydroxy-3-phenoxypropyl acrylate crosslinked with 6.5 mol% *N,N*-methylenebisacrylamide.

compositions with 6 replicates each, yielding a data set with >66.000 measurement points.

To validate the generated data, additional measurements in microliter size were performed. Therefore, four different compositions with clear degradation behavior were chosen and prepolymerization mixtures of the exact same composition were prepared. Polymer pads of 150 µL were polymerized in triplicates under the same conditions as on the slide and swollen in PBS for one week to achieve full swelling. Afterwards, the pads were irradiated with UVC light to initiate degradation, the liquefied part was removed and the mass loss over time was recorded. The relative degradation curves for these pads were compared to the relative degradation curves of the sub-microliter-sized pads and showed a reasonable comparability to identify trends in the high-throughput screening. The microliter-sized gels' degradation curves strongly resemble the measured decrease in fluorescence area for the respective gel very well (**Figure 5**), with a clear differentiation between rapid and slow degradation. This upscaled workflow consumed the same time and more materials for the preparation of four hydrogels with three repetitions compared to the miniaturized screening of >900 materials with six replicates of 130 nL each.

As a final validation and to demonstrate the potential of composition-controlled delayed degradation, we prepared a two-dimensional pattern of three different hydrogel compositions on a DMA slide (**Figure 6**). Each hydrogel pad consisted of 130 nL prepolymerization mixture and after polymerization, the pads were stained with Rhodamine 6G. Upon fluorescence microscopy no clear difference could be observed and the pattern was well hidden. Successive irradiation with UV light started destroying the faster degrading hydrogels, revealing a hidden pattern after 20 min. Through this, the first part of the message became visible, reading "LONG". Further irradiation leads to the degradation of the slower degrading hydrogel pads as well, adding additional information to the message and changing the meaning to "LONGER" (Figure 6A), while keeping the nondegradable hydrogels intact.

The hydrogels that make up the frame are chosen to be stable upon irradiation to ensure the conservation of the information. By this, we created a chemical data storage that could reveal information in a time-dependent manner or with respect to environmental factors. This could not only be of interest for the development of alternative data storage or anti-counterfeiting techniques, but also shows very well the possibilities that open up with a high-throughput material discovery pipeline. Since such easy encoding of information is already possible with just three different materials, more sophisticated systems with higher density of information can become possible when using an abundance of different materials to use the given space more efficiently. Thus, the method shown in this report has a wide field of application and might enable even more versatile applications of both the discovery pipeline as well as the discovered materials in the future.

In order to increase the efficiency of workflow and to demonstrate the full potential of the automated platform for materials design and target-property optimization, we integrated methods of machine learning into the high-throughput screening process, sequentially suggesting new compositions and parameters for hydrogel synthesis. Apart from optimizing (maximize or minimize) droplet size, intensity, and UV degradation, we furthermore performed a more general optimization aiming to increase the range of achievable properties, i.e., initial droplet size and degradation lifetime. We prepared a dataset that correlates composition, i.e., monomer and cross-linker type (plus concentration) with size and relative intensity of the micro-droplets as a function of UV exposure time. Each time series was fitted with

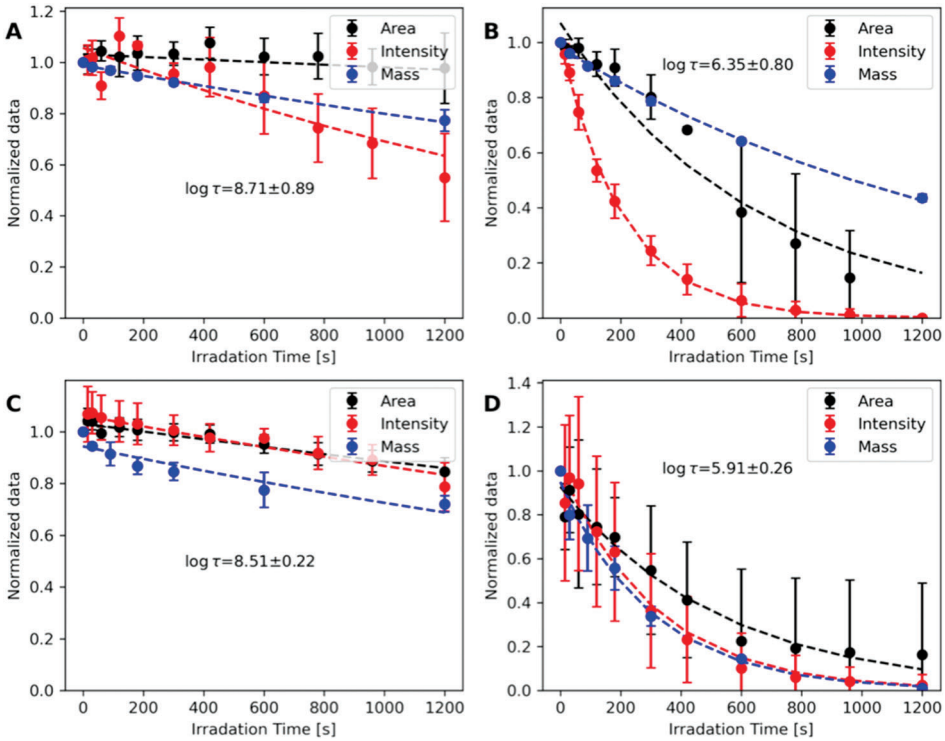

Figure 5. Comparison of degradation curves measured from fluorescence area on sub-microliter scale, fluorescence intensity on sub-microliter scale and mass loss on microliter scale and their respective exponential fits. A) Four types of hydrogels were investigated: mono-2-(methacryloyloxy)ethyl phthalate, crosslinked with 6.5 mol% poly(propylene glycol) dimethacrylate, B) poly(ethylene glycol) methyl ether methacrylate, crosslinked with 6.5 mol% glycerol dimethacrylate, C) 4-hydroxybutyl acrylate, crosslinked with 7.5 mol% trimethylolpropane ethoxylate methyl ether diacrylate, and D) N-(2-acryloyloxyethyl)-N-benzyl-N,N-dimethylammonium chloride, crosslinked with 7.5 mol% trimethylolpropane ethoxylate methyl ether diacrylate. Fluorescence area and integrated intensity are measured from six different 130 nL sized hydrogel pads on DMA, mass loss was measured from three 150 µL sized hydrogel pads polymerized in a PTFE mold. Values in the graphs are the average of the individual repetition's values normalized to the respective repetition value at 0 s irradiation. Error bars show the standard deviation of 6 replicates (nL scale) or 3 replicates (µL scale).

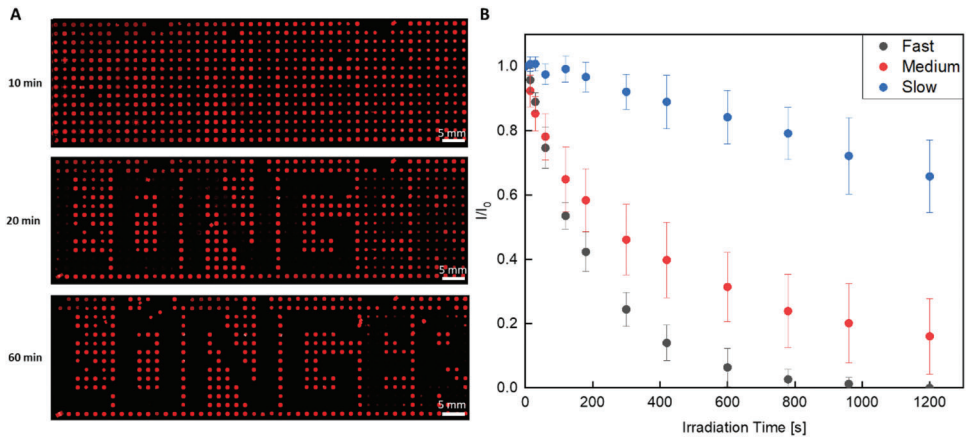

Figure 6. Combination of three different hydrogel compositions with different degradation speeds to create a multilayered data storage. A) Pattern created by polymerization of three different hydrogel types: slow-degradable hydrogel based on 4-hydroxybutyl acrylate and N,N-methylenebisacrylamide (**Slow**), a slightly faster degradable hydrogel made of furfuryl methacrylate and pentaerythritol triacrylate (**Medium**) and a rapidly degradable hydrogel consisting of poly(ethylene glycol)methyl ether acrylate (Mw = 500 Da) and glycerol dimethacrylate (**Fast**). Prior to sufficient irradiation no pattern is visible, after 20 min the word "LONG" becomes visible due to destruction of the fast degradable hydrogels. After further irradiation the slowly degrading hydrogels decompose as well, changing the message to "LONGER". Images have been edited with Adobe Photoshop Lightroom Classic to increase Contrast for better visualization. B) Corresponding degradation curves of the nondegradable composition, slow degrading hydrogels and the rapidly degrading hydrogels. Values shown are measured in a miniaturized screening process and calculated as an average of 6 repetitions normalized to their respective starting value. Error bars shown represent the standard deviation between these six repetitions.

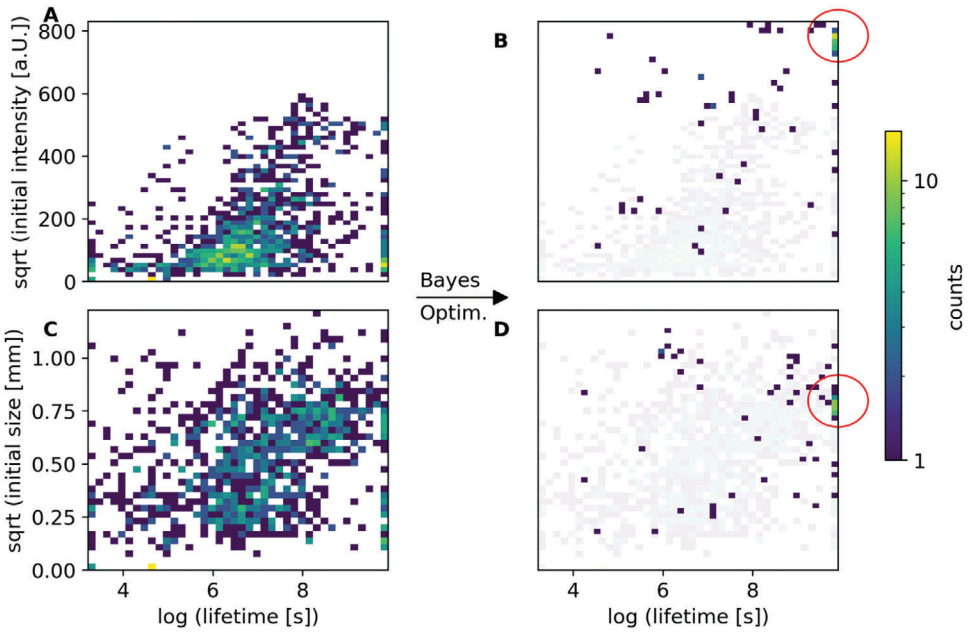

Figure 7. Distribution of all the different hydrogel properties (intensity/size) versus the degradation lifetime before and after Bayesian optimization. 2D histogram of the square root of the A) initial measured average intensity or C) initial size versus the fitted log-lifetime of the hydrogel under UV-irradiation. The 2D histogram after Bayesian optimization of the square root of the B) initial measured average intensity or D) initial size versus the fitted log-lifetime of the hydrogel. Brighter colors represent higher density indicated by a colorbar legend. On the left, the distributions of the initial, randomly selected hydrogels are shown. On the right, the distribution of experimentally measured suggestions from Bayesian optimization (both multiobjective and extremal property search) are shown (with the initial distributions in the background). Red circles in (B) and (D) highlight areas of high lifetime and intensity with multiple compositions.

an exponential decay curve (Equation 1) with initial size/intensity N_0 and mean lifetime.

$$N(t) = N_0\, e^{-t/\tau} \tag{1}$$

To adjust the distribution of target values for ML models, we chose the square root of the initial size and the intensity N_0 of the droplet as well as the natural logarithm of the lifetime τ as learnable targets. Additionally, we clipped the lifetime at $\tau \in [25\text{ s}, 20'000]$ to be within a reasonable value range matching the experimental resolution. The distribution for the randomly generated ≈900 compositions of the high throughput screening is shown in **Figure 7**A,C. Further statistical analysis of the measured values per monomer or cross-linker is shown in Figure S1, Supporting Information, identifying well-performing cross-linker or monomer classes. We trained two multitask Gaussian process regression models (GPR) to predict (a) the combined square root intensity plus log lifetime, and (b) the square root size plus log lifetime from given input compositions. Details about the ML methods are given in Section 4.11. A plot of the prediction of the GPR versus the ground truth can be found in the SI in Figure S2, Supporting Information.

The currently used Gaussian Process models predict hydrogel properties based on monomer and cross-linker class labels and their respective concentration, which implies that they can only be used on a finite set of compounds. In principle, the input representation can be based on molecular features and structural information, rather than categorical compounds, and therefore enable predictions also on unseen monomers. While data requirements for this approach are higher, it would allow for virtual materials design and exploration of new monomers and cross-linkers, which is beyond the scope of this work.

With the Gaussian Process trained on categorical input representations as a surrogate model, we conducted batched Bayesian optimization (BO) cycles to suggest new synthesis parameters. With an expected improvement acquisition function, we maximized the single objective of highest intensity (or size) and longest lifetime. For combined optimization, we define the weighted sum of normalized intensity (or size) and normalized lifetime as objective (normalization constants are the largest values found in the initial screen, details can be found in methods). Additionally, we ran a BO experiment to increase the expected hypervolume of the target space, i.e., find compositions with extremal properties, e.g., maximal intensity and minimal lifetime. The distribution of the measured properties of the newly suggested hydrogels is shown in comparison to the high-throughput screening in Figure 7B,D. Overall we ran two batched BO steps with in total 79 newly suggested hydrogel compositions. In the initial randomized high-throughput screening most monomer to cross-linker combinations were tested, which is why only few new combinations were suggested and mostly the cross-linker concentration and monomer composition parameters were optimized by the BO approach. We find a substantially increased maximum intensity in Figure 7D compared to 7C at all possible lifetimes, while the maximal droplet size is intrinsically limited by the overall printed volume and the area of pad-size on the substrate, not allowing for much further maximization. A bright spot indicates multiple compositions of high lifetime and

intensity as the result of the converged BO suggestions, marked by a red circle in Figure 7B,D. Moreover, additional compositions in previously underexplored regions are found, e.g. large and fast degrading droplets, upper left corner of Figure 7A.

3. Summary and Conclusion

Droplet microarray is a platform which was previously proven to be very versatile for chemical synthesis, cell culture, or drug screening. In this work, we demonstrated the possibility to expand the scope of DMA setups into a smart, miniaturized, high throughput materials discovery platform. We transitioned from small libraries with known behavior to large chemical spaces including thousands of different, unknown polymeric compositions. The versatility of the platform allowed these adjustments to the experimental workflow to fit a broad scope of different functionalities, enabling the high-throughput synthesis and analysis of various different materials while maintaining a minimal material consumption. The synthesis and screening of the first 918 different compositions with six replicates (for a total of 5508 experiments) was performed in a short time window of one week while consuming only 551 µL of highly diluted monomer stock solutions. For comparison, the validation experiment of four compositions in triplicates consumed roughly 2.5 times the amount of material needed for the whole miniaturized screening, while taking already more time to just swell the larger gel pads than the whole screening pipeline. To perform the whole screening within this scale, the total material consumption would be 574 times higher (316 mL). This shows the advantages of miniaturization and parallelization compared to conventional analysis methods and establishes the DMA once again as a very versatile and applicable platform. The automatic experiment platform for hydrogels can be further combined with Bayesian optimization to further optimize target properties of interest or to explore and expand the space of achievable materials properties. We demonstrated that Bayesian optimization can find hydrogel compositions that increase intensity and lifetime substantially beyond what was found in the initial random screening process.

Controlling photodegradation lifetime of soft materials is of interest for different applications, such as the design of anisotropically degrading scaffolds for 3D cell culture. The coverage of different property combinations achieved in the initial screening (Figure 7A/C) was further expanded after the optimization step, thus gaining access to new subsets of materials with useful properties, such as low lifetime and high initial intensity (Figure 7B). Herein discovered materials with comparable size and therefore comparable swelling behavior can be used for the fabrication of multimaterial structures that keep their structural features independent of their swelling degree. Thus, combinations of these materials with matching properties can easily be used for encryption of information into hidden patterns, only visible upon irradiation (Figure 6), as data storage, as a degradable scaffold, or as hydrogel-based photoresists for lithography. Furthermore, insights into their UV-driven degradation might allow the use of methacrylates as naturally decomposing polymers upon exposure to sunlight.

Beyond that, with the possibility to reliably produce materials in the sub-microliter range, one can in principle gain access to any other materials property which is measurable in a miniaturized setup. Smart high-throughput optimization of composition and synthesis parameters, enables the design of materials with, e.g., tailormade biocompatibility through measurement of cell viability assays, mechanical properties through integration of miniaturized mechanosensors, or drug/biomolecule loading capacities through characterization by fluorescence microscopy. Accessing more and more research areas with miniaturized approaches coupled to machine learning algorithms is one of the most promising ways to achieve sustainable and future-oriented research practices.

4. Experimental Section

Droplet Microarray: The preparation of Droplet Microarrays was done according to a patented procedure.[46] For the preparation uncoated Nexterion glass slides (Schott AG, Mainz, Germany) were used. The glass was activated prior to use by 10 min ozone treatment in an UVO-Cleaner (Jetlight Co. Inc., Irvine, CA). Afterward the slides were coated with a solution of AEROSIL 200 (Evonik Industries AG, Essen, Germany), trimethoxyvinylsilane (VWR International, Radnor, PA), and hydrochloric acid (VWR International, Radnor, PA) in ethanol (VWR International, Radnor, PA). Slides were cured at 150 °C for an hour and then washed with ethanol. For the creation of hydrophobic or hydrophilic regions slides were covered with a solution or 1H,1H,2H,2H-perfluorodecanethiol in isopropanol or mercaptoethanol in ethanol/water (1:1) respectively, and irradiated for 90 s using a UVA Cube 2000 (Dr. Hönle AG, Gilching, Germany).

Monomers: The Monomers used in the library synthesis were chosen to cover diverse different functionalities to achieve both structurally very similar and very different polymeric compositions. methacrylamide, hydroxypropyl methacrylate, diacetone acrylamide, N,N-dimethylacrylamide, hydroxypropyl acrylate, N-(3-dimethylaminopropyl)methacrylamide, 1-(acryloyloxy)-3-(methacryloyloxy)-2-propanol, methoxyethyl acrylate, 3-chloro-2-hydroxypropyl methacrylate, diethylene glycol monomethyl ether methacrylate, N-(butoxymethyl)acrylamide, 2-methoxyethyl methacrylate, tetrahydrofurfuryl acrylate, 2-(diethylamino)ethyl acrylate, 2-hydroxy-3-phenoxypropyl acrylate, 4-hydroxybutyl acrylate, 2-acrylamido-2-methylpropanesulfonic acid, 2-(dimethyl)ethyl acrylate, glycerol dimethacrylate, mono(2-acryloyloxyethyl) succinate, 3-Sulfopropyl acrylate potassium salt, 4-acryloylmorpholine, mono-2-(methacryloyloxy)ethyl phtalate, N-(2-acryloyloxyethyl)-N-benzyl-N,N-dimethylammonium chloride, alpha-methylene-gamma-butyrolactone, *N*-methylmethacrylamide, 2-(methacryloyloxy)ethyl 2-(trimethylammonio)ethyl phosphate, 2-morpholinoethyl methacrylate, furfuryl methacrylate, *N*-isopropylmethacrylamide, methacrolein, *N*-(3-aminopropyl)methacrylamide hydrochloride, 4-[(3-methacrylamidopropyl)dimethylamonio]butane-1-sulfonate, N-(3-dimethylaminopropyl)methacrylamide were purchased from TCI (Tokyo, Japan). 1,12-dodecandiol dimethacrylate was purchased from abcr GmbH(Karlsruhe, Germany), 2-aminoethyl methacrylate hydrochloride, pentaerythritol triacrylate, diethylene glycol diacrylate, N,N-dimethylacrylamide, methyl methacrylate, propargyl methacrylate, 2-hydroxyethyl acrylate, cyclohexyl methacrylate was purchased from Thermo Fischer Scientific Inc. (Waltham, MA), ethylene glycol dimethacrylate, tri(ethylene glycol) dimethacrylate, di(ethylene glycol)dimethacrylate, poly(ethylene glycol) dimethacrylate (Mn ~ 750 Da), poly(propylenglykol)dimethacrylate, trimethylolpropane trimethacrylate, poly(ethylene glycol)diacrylate (Mn ~ 700 Da), poly(ethylene glycol)diacrylate (Mn ~ 575 Da), poly(ethylene glycol) diacrylate (Mn ~ 250 Da), 1,4-butanediol diacrylate, glycerol 1,3-diglycerolate diacrylate, trimethylolpropane ethoxylate (1 EO/OH) methyl ether diacrylate, N,N′-methylenebisacrylamide, N,N′-(1,2-dihydroxyethylene)bisacrylamide, acrylamide, N-isopropylacrylamide, poly(ethylene glycol)methyl ether acrylate (Mn ~ 480 Da), poly(ethylene glycol)methyl ether methacrylate (Mn ~ 500 Da), glycidyl methacrylate, 2-hydroxyethyl methacrylate, lauryl methacrylate, butyl methacrylate, ferrocenyl methacrylate,

2-(dimethylamino)ethyl methacrylate, isobornyl methacrylate, poly(ethylene glycol) methyl ether methacrylate (Mn = 300 Da), 3-sulfopropyl methacrylate potassium salt, isodecyl acrylate, butylacrylate, octadecyl acrylate, methyl acrylate, [2-(methacryloyloxy)ethyl]-dimethyl-(3-sulfopropyl)-ammonium hydroxide and methacrylic acid were bought from Sigma Aldrich (St. Louis, MO).

Printing: Monomers were purified from inhibitors prior to use by passing over a column of basic aluminum oxide (Alfa Aesar, Ward Hill, MA, USA). For dispensing a Certus Flex (Fritz Gyger AG, Gwatt, Switzerland) was used, viscosity of printing solutions was adjusted and calibrated to assure reproducible and precise printing.

In a typical printing procedure 130 nL PBS (Thermo Fisher Scientific Inc., Waltham, MA) were dispensed to the outer frame of the droplet microarray to make sure every gel containing spot will be surrounded by other gel-containing spots or humidifying rows containing PBS. Then 30 nL lithium phenyl-2,4,6-trimethylbenzoylphosphinate (Sigma-Aldrich, St. Louis, MO) solution (5 mg mL^{-1}) in PBS, supplemented with glucose oxidase (40 µM) (VWR International, Radnor, PA) and glucose (0.1 M) (Sigma-Aldrich, St. Louis, MO) were dispensed into the inner spots. 60 nL of monomer solution (1.66 M) and 30 nL cross-linker solution (0.581 M) in PBS or DMF were added subsequently. For larger libraries, the slide was stored on a metal cooling plate at 0 °C during the exchange of stock solutions to fully suppress evaporation-induced concentration changes.

Polymerization: After printing the slides containing prepolymerization mixture were transferred into a petri dish containing 2 mL PBS in the bottom, covered with a quartz glass plate, and irradiated for 30 min with a UV LED (Opsytec, Ettlingen, Germany) at 5.41 mW cm^{-2}. After the polymerization Slides were taken out of the dish and submerged in a solution of Rhodamine 6G (10 mg L^{-1}) in PBS for 16 h.

Photodegradation on Sub-Microliter Scale: Swollen hydrogel pads were taken out of solution, excess solvent was carefully removed and the slide was sealed with a PDMS frame stuck to a quartz glass slide. The sealed slide was irradiated with the quartz glass slide pointing towards the light source. As UV source a UVA Cube 2000 (Dr. Hönle AG, Gilching, Germany) was used (11.45 mW cm^{-2}). and with a regular frequence imaged by fluorescence microscopy on a Keyence BZ-X800 with a 2X magnification lense (Keyence Co., Ösaka, Japan) in the TRITC channel (Excitation 544 nm, Emission 570 nm) at 4 ms excitation time. The recorded images were segmented and analyzed to determine the fluorescence area and the integrated intensity of every single pad.

Preparation of Prepolymerization Mixtures on Microliter Scale: To a solution of monomer (0.89 M) and crosslinker (from 5 to 15 mol% w.r.t. Monomer) in PBS and DMF, LAP was added (1.13 mg m L^{-1}). Nitrogen was bubbled through the mixture for 15 min to remove oxygen, then the Prepolymerization mixture was ready to use for the following experiments.

Photodegradation on Microliter Scale: The hydrogels for this were prepared by dispensing 150 µL prepolymerization mixture into an PTFE mold, which was then covered with a quartz glass plate and irradiated according to the polymerization protocol. The gel pads were taken out of the mold and submerged in PBS for 7 days to achieve full swelling. Samples were taken out and dried of excess water using tissues. The samples were irradiated in a close petri dish with 2 mL PBS in the bottom under the same conditions as for the sub-microliter degradation studies. After specific time intervals, the samples were taken out, liquefied parts were removed again and the sample was weighed. The mass change was measured over 20 min and the mass was normalized to the starting mass to generate the course of degradation. For every measurement, three independent repetitions were performed.

Preparation of Irradiation Time-dependent Patterns: Prepolymerization mixtures for the three different compositions were prepared and dispensed onto a DMA slide. Each spot confined a volume of 130 nL prepolymerization mixture. The polymerization was done according to the Polymerization protocol and the slides were afterward submerged in Rhodamine 6G solution in PBS (10 mg L^{-1}). After 24 h, the slides were taken out, excess water was removed with a tissue and the slides were imaged with a fluorescence microscope (1.25 ms excitation time). Slides were irradiated in a petri dish sealed with a quartz glass plate for 10 min using UVC light and afterward washed by carefully immersing in PBS for a moment. Slides were taken out, excess water was removed with a tissue and the slides were imaged again. This was repeated for every desired irradiation time.

Intensity Measurements: UVA- or UVC intensities of all lamps were measured with a UV-Meter (Dr. Hönle AG, Gräfelfing, Germany) using an UVA- or UVC-sensor respectively.

Image Analysis: Fluorescence microscopy images were evaluated with an in-house developed software tool for automatic droplet grid- and edge-detection, featuring a graphical user interface for supervision and adjustment. The code is available at https://github.com/aimat-lab/microdroplet_segmentation. For edge detection, a sobel filter with median and gaussian blurring from scikit-image was chosen.[47,48] After droplet segmentation with a two-label watershed algorithm within each array box on the sobel elevation map,[49–51] the pixel size and integrated gray-scale intensities of each droplet were recorded.

Machine Learning: Each time series of the UV degradation curve was fitted with an exponential function with 2 parameters, from which the labels of lifetime and initial size and intensity were obtained. The data for the training of the ML models by taking the square root of initial size and intensity and the logarithm of the lifetime were prepared. Additionally, the lifetime at $\tau \in [25\ s,\ 20'000\ s]$ was clipped. A multitask Gaussian process regressor (GPR) as implemented in GPyTorch[52] to train on a random seven-fold split was used. The output space of the multi-task GPR is 4-dimensional, i.e., initial square root intensity and size as well as their respective log-lifetimes. Mixed inputs of two categorical class labels for monomer and crosslinker and a continuous parameter of their molar concentrations were used. Alternatively class labels can be mapped into one-hot encoded monomer and cross-linker vectors of combined 75 dimensions. Fit results are summarized in Figure S2, Supporting Information.

Bayesian Optimization: Batched Bayesian Optimization with both the Ax[53] and BOTorch[54] library in a single and multitarget configuration was performed. For the single task setting, the objective was set to be the sum or difference of normalized lifetime and normalized initial size (or average intensity). For the mult-label settings, the objective was set to maximize the space of all labels. For BOTorch a *MixedSingleTaksGP* with *SobolQMCNormalSampler* and *qExpectedImprovement* for optimization in the single target setting were chosen. A list of *MixedSingleTaksGP* with *qNoisyExpectedHypervolumeImprovement* in the multitarget setting. For Ax, the Service API was used and skipped the initial suggestion. All predictions of the different approaches were combined for the next experimental measurement round.

Creation of Figures: The creation of Figure 1 and the table of contents Figure was done with Biorender.com.

Supporting Information

Supporting Information is available from the Wiley Online Library or from the author.

Acknowledgements

M.S. and P.R. contributed equally to this work. This project was partly supported by DFG (Heisenbergprofessur Projektnummer: 406232485, LE 2936/9-1). Furthermore, the authors thank the Helmholtz Program "Materials Systems Engineering" for the support.

Open access funding enabled and organized by Projekt DEAL.

Conflict of Interest

The authors declare no conflict of interest.

Data Availability Statement

The data that support the findings of this study are available from the corresponding author upon reasonable request.

Keywords

bayesian optimization, high throughput, hydrogels, machine learning, materials acceleration platforms, stimuli-responsiveness

Received: April 27, 2023
Published online:

[1] S. C. Lee, I. K. Kwon, K. Park, *Adv. Drug Delivery Rev.* **2013**, *65*, 17.
[2] S. Guragain, B. P. Bastakoti, V. Malgras, K. Nakashima, Y. Yamauchi, *Chemistry* **2015**, *21*, 13164.
[3] P. P. Shinde, S. Shah, *In 2018 Fourth International Conference on Computing Communication Control and Automation (ICCUBEA)*, IEEE, Piscataway, NJ **2018**, 603.
[4] S. Lu, Q. Zhou, Y. Ouyang, Y. Guo, Q. Li, J. Wang, *Nat. Commun.* **2018**, *9*, 3405.
[5] G. Pilania, A. Mannodi-Kanakkithodi, B. P. Uberuaga, R. Ramprasad, J. E. Gubernatis, T. Lookman, *Sci. Rep.* **2016**, *6*, 19375.
[6] K. Kim, S. Kang, J. Yoo, Y. Kwon, Y. Nam, D. Lee, I. Kim, Y.-S. Choi, Y. Jung, S. Kim, W.-J. Son, J. Son, H. S. Lee, S. Kim, J. Shin, S. Hwang, *NPJ Comput. Mater.* **2018**, *4*, 67.
[7] J. Schmidt, M. R. G. Marques, S. Botti, M. A. L. Marques, *NPJ Comput. Mater.* **2019**, *5*, 83.
[8] P. Raccuglia, K. C. Elbert, P. D. F. Adler, C. Falk, M. B. Wenny, A. Mollo, M. Zeller, S. A. Friedler, J. Schrier, A. J. Norquist, *Nature* **2016**, *533*, 73.
[9] B. Liu, B. Ramsundar, P. Kawthekar, J. Shi, J. Gomes, Q. Luu Nguyen, S. Ho, J. Sloane, P. Wender, V. Pande, *ACS Cent. Sci.* **2017**, *3*, 1103.
[10] M. H. S. Segler, M. Preuss, M. P. Waller, *Nature* **2018**, *555*, 604.
[11] C. W. Coley, W. H. Green, K. F. Jensen, *Acc. Chem. Res.* **2018**, *51*, 1281.
[12] E. Sotillo, D. M. Barrett, K. L. Black, A. Bagashev, D. Oldridge, G. Wu, R. Sussman, C. Lanauze, M. Ruella, M. R. Gazzara, N. M. Martinez, C. T. Harrington, E. Y. Chung, J. Perazzelli, T. J. Hofmann, S. L. Maude, P. Raman, A. Barrera, S. Gill, S. F. Lacey, J. J. Melenhorst, D. Allman, E. Jacoby, T. Fry, C. Mackall, Y. Barash, K. W. Lynch, J. M. Maris, S. A. Grupp, A. Thomas-Tikhonenko, *Cancer Discovery* **2015**, *5*, 1282.
[13] M. K. K. Leung, H. Y. Xiong, L. J. Lee, B. J. Frey, *Bioinformatics* **2014**, *30*, i121.
[14] H. Y. Xiong, B. Alipanahi, L. J. Lee, H. Bretschneider, D. Merico, R. K. C. Yuen, Y. Hua, S. Gueroussov, H. S. Najafabadi, T. R. Hughes, Q. Morris, Y. Barash, A. R. Krainer, N. Jojic, S. W. Scherer, B. J. Blencowe, B. J. Frey, *Science* **2015**, *347*, 1254806.
[15] K. P. Mishra, L. Ganju, M. Sairam, P. K. Banerjee, R. C. Sawhney, *Biomed. Pharmacother.* **2008**, *62*, 94.
[16] A. D. Rouillard, M. R. Hurle, P. Agarwal, *PLoS Comput. Biol.* **2018**, *14*, e1006142.
[17] S. Riniker, Y. Wang, J. L. Jenkins, G. A. Landrum, *J. Chem. Inf. Model.* **2014**, *54*, 1880.
[18] F. Iorio, T. A. Knijnenburg, D. J. Vis, G. R. Bignell, M. P. Menden, M. Schubert, N. Aben, E. Gonçalves, S. Barthorpe, H. Lightfoot, T. Cokelaer, P. Greninger, E. van Dyk, H. Chang, H. de Silva, H. Heyn, X. Deng, R. K. Egan, Q. Liu, T. Mironenko, X. Mitropoulos, L. Richardson, J. Wang, T. Zhang, S. Moran, S. Sayols, M. Soleimani, D. Tamborero, N. Lopez-Bigas, P. Ross-Macdonald, et al., *Cell* **2016**, *166*, 740.
[19] P. K. Donepudi, *J. Adv. Res.* **2018**, *7*, 109.
[20] R. Gómez-Bombarelli, J. Aguilera-Iparraguirre, T. D. Hirzel, D. Duvenaud, D. Maclaurin, M. A. Blood-Forsythe, H. S. Chae, M. Einzinger, D.-G. Ha, T. Wu, G. Markopoulos, S. Jeon, H. Kang, H. Miyazaki, M. Numata, S. Kim, W. Huang, S. I. Hong, M. Baldo, R. P. Adams, A. Aspuru-Guzik, *Nat. Mater.* **2016**, *15*, 1120.
[21] B. P. MacLeod, F. G. L. Parlane, T. D. Morrissey, F. Häse, L. M. Roch, K. E. Dettelbach, R. Moreira, L. P. E. Yunker, M. B. Rooney, J. R. Deeth, V. Lai, G. J. Ng, H. Situ, R. H. Zhang, M. S. Elliott, T. H. Haley, D. J. Dvorak, A. Aspuru-Guzik, J. E. Hein, C. P. Berlinguette, *Sci. Adv.* **2020**, *6*, eaaz8867.
[22] S. Langner, F. Häse, J. D. Perea, T. Stubhan, J. Hauch, L. M. Roch, T. Heumueller, A. Aspuru-Guzik, C. J. Brabec, *Adv. Mater.* **2020**, *32*, 1907801.
[23] B. J. Shields, J. Stevens, J. Li, M. Parasram, F. Damani, J. I. M. Alvarado, J. M. Janey, R. P. Adams, A. G. Doyle, *Nature* **2021**, *590*, 89.
[24] P. Reiser, M. Neubert, A. Eberhard, L. Torresi, C. Zhou, C. Shao, H. Metni, C. van Hoesel, H. Schopmans, T. Sommer, P. Friederich, *Commun. Mater.* **2022**, *3*, 93.
[25] A. McGovern, R. Lagerquist, D. J. Gagne, G. E. Jergensen, K. L. Elmore, C. R. Homeyer, T. Smith, *Bull. Am. Meteorol. Soc.* **2019**, *100*, 2175.
[26] S. M. Moosavi, K. M. Jablonka, B. Smit, *J. Am. Chem. Soc.* **2020**, *142*, 20273.
[27] M. Krenn, R. Pollice, S. Y. Guo, M. Aldeghi, A. Cervera-Lierta, P. Friederich, G. dos Passos Gomes, F. Häse, A. Jinich, A. Nigam, Z. Yao, A. Aspuru-Guzik, *Nat. Rev. Phys.* **2022**, *4*, 761.
[28] F. Tamaki, F. Fisher, R. Milne, F. S.-R. Terán, N. Wiedemar, K. Wrobel, D. Edwards, H. Baumann, I. H. Gilbert, B. Baragana, J. Baum, S. Wyllie, *Antimicrob. Agents Chemother.* **2022**, *66*, e0023722.
[29] K. Ning, A. Roy, F. Cheng, P. Xu, S. Kleiboeker, C. R. Escalante, J. Wang, J. Qiu, *J. Virol.* **2022**, *96*, e0132621.
[30] D. Mav, R. R. Shah, B. E. Howard, S. S. Auerbach, P. R. Bushel, J. B. Collins, D. L. Gerhold, R. S. Judson, A. L. Karmaus, E. A. Maull, D. L. Mendrick, B. A. Merrick, N. S. Sipes, D. Svoboda, R. S. Paules, *PLoS One* **2018**, *13*, e0191105.
[31] G. Ates, B. Mertens, A. Heymans, L. Verschaeve, D. Milushev, P. Vanparys, N. H. C. Roosens, S. C. J. De Keersmaecker, V. Rogiers, T. Y. Doktorova, *Arch. Toxicol.* **2018**, *92*, 1593.
[32] J. M. Yeakley, P. J. Shepard, D. E. Goyena, H. C. VanSteenhouse, J. D. McComb, B. E. Seligmann, *PLoS One* **2017**, *12*, e0178302.
[33] K. Y. Lee, D. J. Mooney, *Chem. Rev.* **2001**, *101*, 1869.
[34] Y. Lee, W. J. Song, J.-Y. Sun, *Mater. Today Phys.* **2020**, *15*, 100258.
[35] C. B. Goy, R. E. Chaile, R. E. Madrid, *React. Funct. Polym.* **2019**, *145*, 104314.
[36] H. Kamata, X. Li, U. Chung, T. Sakai, *Adv. Healthcare Mater.* **2015**, *4*, 2360.
[37] M. Villiou, J. I. Paez, A. del Campo, *ACS Appl. Mater. Interfaces* **2020**, *12*, 37862.
[38] J. M. Scheiger, S. Li, M. Brehm, A. Bartschat, P. Theato, P. A. Levkin, *Adv. Funct. Mater.* **2021**, *31*, 2105681.
[39] A. Rosenfeld, T. Göckler, M. Kuzina, M. Reischl, U. Schepers, P. A. Levkin, *Adv. Healthcare Mater.* **2021**, *10*, 2100632.
[40] A. Rosenfeld, C. Oelschlaeger, R. Thelen, S. Heissler, P. A. Levkin, *Mater. Today Bio.* **2020**, *6*, 100053.
[41] W. Feng, L. Li, E. Ueda, J. Li, S. Heißler, A. Welle, O. Trapp, P. A. Levkin, *Adv. Mater. Interfaces* **2014**, *1*, 1400269.
[42] W. Lei, A. Deckers, C. Luchena, A. Popova, M. Reischl, N. Jung, S. Bräse, T. Schwartz, I. K. Krimmelbein, L. F. Tietze, P. A. Levkin, *Adv Biol* **2022**, *6*, 2200166.
[43] Y. Liu, S. Bertels, M. Reischl, R. Peravali, M. Bastmeyer, A. A. Popova, P. A. Levkin, *Adv. Healthcare Mater.* **2022**, *11*, 2200718.
[44] A. Rosenfeld, M. Brehm, A. Welle, V. Trouillet, S. Heissler, M. Benz, P. A. Levkin, *Mater. Today Bio.* **2019**, *3*, 100022.
[45] M. Brehm, S. Heissler, S. Afonin, P. A. Levkin, *Small* **2020**, *16*, 1905971.
[46] P. A. Levkin, M. Grunze, Z. Dong, K. Demir, S. Widmaier, M. Brehm, A. Popova, *EP 3733277*, **2020**.

[47] G. Bradski, A. Kaehler, *Learning OpenCV: Computer Vision with the OpenCV Library*, O'Reilly Media, Inc., Sebastopol, California **2008**.
[48] S. van der Walt, J. L. Schönberger, J. Nunez-Iglesias, F. Boulogne, J. D. Warner, N. Yager, E. Gouillart, T. Yu, *PeerJ* **2014**, *2*, e453.
[49] F. Pedregosa, G. Varoquaux, A. Gramfort, V. Michel, B. Thirion, O. Grisel, M. Blondel, P. Prettenhofer, R. Weiss, V. Dubourg, J. Vanderplas, A. Passos, D. Cournapeau, M. Brucher, M. Perrot, É. Duchesnay, *J. Mach Learn Res.* **2011**, *12*, 2825.
[50] J. D. Hunter, *Comput. Sci. Eng.* **2007**, *9*, 90.
[51] P. Neubert, P. Protzel, *In 2014 22nd International Conference on Pattern Recognition*, IEEE, Piscataway, NJ **2014**, pp. 996.
[52] J. R. Gardner, G. Pleiss, D. Bindel, K. Q. Weinberger, A. G. Wilson, *In Proceedings of the 32nd International Conference on Neural Information Processing Systems*, Curran Associates Inc., Red Hook, NY, USA, **2018**, pp. 7587.
[53] D. T. Chang, **2019**, https://doi.org/10.48550/arXiv.1912.05686.
[54] M. Balandat, B. Karrer, D. R. Jiang, S. Daulton, B. Letham, A. Wilson, E. Bakshy, **2020**, https://doi.org/10.48550/arXiv.1910.06403.

